Article

Oxygen Exchange on Vanadium Pentoxide

Yuanqing Wang, Frank Rosowski, Robert Schlögl, and Annette Trunschke*
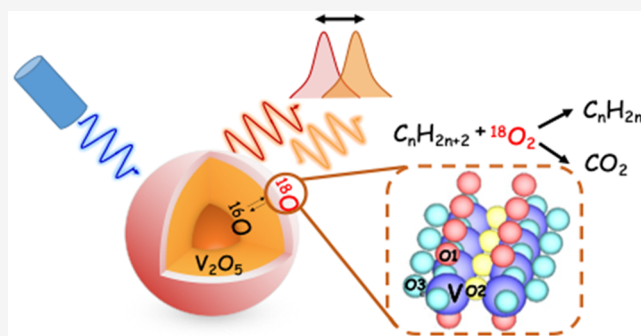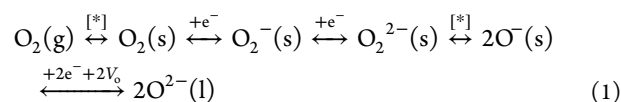
Read Online

ACCESS | 📊 Metrics & More | 📑 Article Recommendations | 🔲 Supporting Information

ABSTRACT: The isotopic exchange of $^{18}O_2$ on polycrystalline $V_2{}^{16}O_5$ was studied by Raman spectroscopy at different temperatures between 300 and 580 °C and in the presence of different mixtures of oxygen with ethane, propane, or *n*-butane in the gas phase. Supported by DFT calculations, a method was developed to determine which of the three differently coordinated oxygen atoms in the crystal structure of V_2O_5 (vanadyl oxygen O1, 2-fold-coordinated oxygen O2, and three-coordinated oxygen O3) are involved in the exchange with $^{18}O_2$ from the gas phase. Thus, it was found that the band at 994 cm^{-1}, which is commonly exclusively assigned to a V=^{16}O1 stretching (A_g) vibration, also contains contributions of an ^{16}O1−V−^{16}O2 stretching vibration (B_{2g}). If only the O1 position is exchanged, the B_{2g} component shifts to 964.2 cm^{-1}, while if both O1 and O2 are exchanged, a shift to 953.4 cm^{-1} is expected. In contrast, the A_g component shifts only to 955 cm^{-1}, regardless of whether only the O1 position or all three oxygen atoms are exchanged. On this basis, it was found that oxygen exchange at 573 °C in absence of an alkane involves O1 and O3 atoms, whereas in the presence of propane all three oxygen atoms are exchanged. In the latter case, the overall exchange rate appears to be limited by bulk diffusion. At typical reaction temperatures for the oxidative dehydrogenation of propane between 320 and 430 °C, no exchange occurs in pure oxygen. In presence of ethane or propane, only O1 is partly exchanged possibly at the surface and/or in a near-surface region. Under the typical reaction conditions of oxidative dehydrogenation of propane at 400 °C, there is hardly any variation in the spectra, and the small changes observed after long times on stream only affect O1, which, considering the sensitivity of the measurement method, leaves open whether the Mars−van Krevelen mechanism is indeed the predominant reaction mechanism under the conditions of oxidative dehydrogenation of alkanes on V_2O_5.

1. INTRODUCTION

Activation of molecular oxygen on the surface of metal oxides is of fundamental importance in heterogeneous catalysis,[1−3] solid oxide fuel cells,[4] and gas sensor technology.[5] Direct oxidation of inert alkane molecules with gas-phase oxygen over metal oxide catalysts not only is of economic interest but poses a challenge in scientific understanding due to the complexity of the catalysts as well as the reaction networks.[6] The selective oxidation of alkanes requires both the activation of C−H bonds in the alkane molecule and the activation of molecular oxygen. Reactive oxygen species formed in the process of charge transfer between the hydrocarbon and the oxygen molecule include electrophilic or nucleophilic intermediates, respectively. The process of O_2 dissociation and final incorporation of oxygen into the oxide lattice involves the polarized adsorbed O_2 molecule, differently adsorbed charged molecular species (superoxide $O_2{}^-$ and peroxide $O_2{}^{2-}$), and charged atomic species (O^-) with electrophilic character. The reaction ultimately leads to the incorporation of nucleophilic O^{2-} ions into the lattice (eq 1),[7]

$$O_2(g) \overset{[*]}{\leftrightarrow} O_2(s) \xrightarrow{+e^-} O_2{}^-(s) \xrightarrow{+e^-} O_2{}^{2-}(s) \overset{[*]}{\leftrightarrow} 2O^-(s)$$
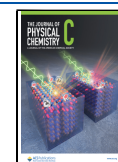$$\xrightarrow{+2e^- + 2V_o} 2O^{2-}(l) \tag{1}$$

where the symbols * stand for a free adsorption site, g for gas phase, s for surface, and l for lattice. It was discussed that surface and volume defects are important for both adsorption and dissociation of oxygen.[8−13]

Control over the occurrence and distribution of the different oxygen species under the reaction conditions is key to achieving high selectivity for certain reaction products and avoiding complete combustion to unwanted CO_2 during alkane oxidation. Different types of oxygen species are required depending on whether an olefin is to be formed by oxidative hydrogen abstraction or whether oxygenates are the desired products. The synthesis of oxygenates containing C−C double
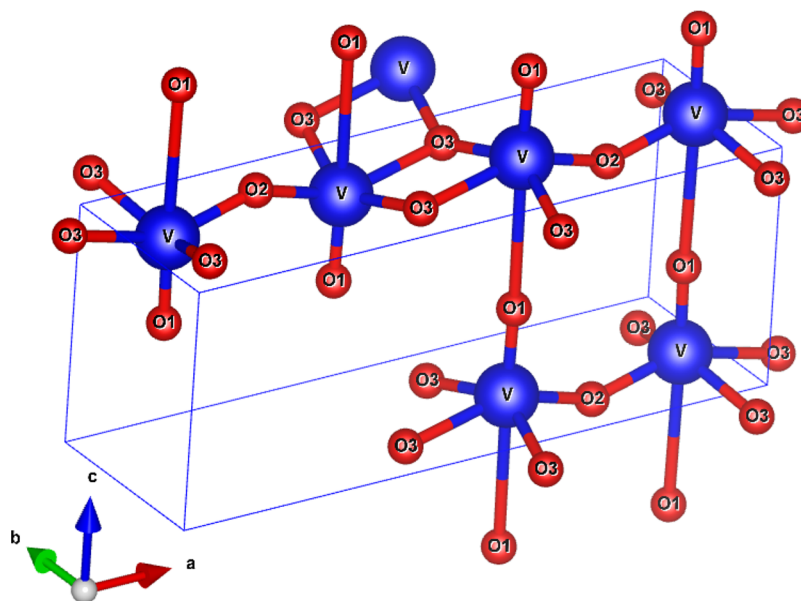
Figure 1. Unit cell of V_2O_5: O1, terminal oxygen; O2, bridging oxygen; O3, chain oxygen.

bonds requires the simultaneous presence of nucleophilic and electrophilic oxygen species, which can coexist at different locations on the catalyst surface. Ultimately, it is a matter of avoiding total oxidation to carbon dioxide, which is also the product of oxygen incorporation and C−C bond cleavage.

Experimental discrimination of oxygen species actually involved in hydrocarbon oxidation is complicated due to the elevated reaction temperatures that lead to rapid interconversion of the intermediates, which appear in eq 1.[1] Furthermore, the low concentration of active sites,[14,15] the limited sensitivity of suitable spectroscopic techniques such as vibrational[16] and EPR spectroscopies, or the superposition of a multitude of oxygen species in photoelectron spectra of working catalysts[17−19] pose additional challenges.[20,21]

Isotope exchange experiments were used to investigate oxygen exchange between the gas phase and oxides under various conditions.[22,23] Three different types of oxygen exchange reactions are distinguished in the postulated mechanisms. The R^0 mechanism does not involve lattice oxygen (M−O_L), but gas-phase $^{16}O_2$ exchanges one oxygen atom with gas-phase $^{18}O_2$ under formation of mixed $^{16}O^{18}O$, while the atomic fraction of the two oxygen isotopes in the gas phase remains constant. In the R^1 and R^2 exchange mechanisms, one or two ^{16}O lattice oxygen atoms, respectively, participate under formation of $^{16}O^{18}O$ and $^{16}O_2$, respectively, in the presence of $^{18}O_2$ in the gas phase. Winter,[24,25] Nováková et al.,[22,26] and Boreskov[27] derived expressions to distinguish the exchange type based on the exchange rate. V_2O_5 was found to follow a combination of R^1 (in the lower temperature range of 480−540 °C) and R^2 (in the higher temperature range of 520−600 °C) mechanism.[25] In other works, only the R^2 mechanism was found above 450 °C.[28,29] Over supported vanadium oxides catalysts the R^2 activity decreases in the order $V_2O_5/TiO_2 > V_2O_5/Al_2O_3 \sim V_2O_5/SiO_2$, which corresponds to the order in which the activity in butane oxidation decreases.[28,30] However, the R^2 activity cannot be solely attributed to surface vanadia species, because ^{17}O NMR provided evidence for participation of the oxygen from the support in the exchange mechanism,[31] suggesting that oxygen exchange rate and reactivity are not necessarily linked. Based

on density functional theory (DFT) calculations, the involvement of a surface ozonide complex O_3^- in the R^1 mechanism, and a 4-atom complex with the O_2^- and O_2^{2-} surface species in the R^2 mechanism over VO_x/TiO_2, respectively, were proposed.[32,33] Some authors indicated that the presence of a reducing gas or the degree of reduction of the oxide has an impact on the oxygen exchange.[29,34]

Kinetic measurements of oxygen exchange, however, do not disclose which lattice oxygen is involved in the exchange. Three different types of oxygen atoms can be distinguished in bulk V_2O_5: (1) vanadyl oxygen O1; (2) 2-fold-coordinated oxygen O2; (3) three-coordinated oxygen O3 (Figure 1). The combination of oxygen exchange with vibrational spectroscopy provides the opportunity to distinguish the type of oxygen that participates in the exchange mechanism. In addition, another disadvantage of the purely kinetic studies of oxygen exchange is eliminated, since the vibrational spectroscopic experiments can usually be carried out *in situ* and not in vacuum and in the absence of alkanes.

In early studies, Hirota and Kera et al. investigated the oxygen exchange between gaseous $C^{18}O_2$ or $^{18}O_2$ over V_2O_5 by infrared spectroscopy.[35−37] A new band appearing at 962 cm^{-1} was ascribed to the V=^{18}O1 stretching in contrast to V=^{16}O1 at 1019 cm^{-1}, however, the low resolution of the infrared spectra complicated the identification of other vibrational modes, which might be simultaneously present.

Raman spectroscopy is a versatile tool in analyzing the interaction of O_2 with metal oxides, because the stretching frequency of molecular oxygen species, which can be measured directly, decreases with decreasing bond order caused by increasing charge transfer from 1556 cm^{-1} for the free oxygen molecule[38] to 1200−1000 cm^{-1} for superoxide and 1000−800 cm^{-1} for peroxide species adsorbed on metal oxide surfaces.[39−41] Furthermore, Raman spectroscopy in combination with theory and isotope exchange experiments has been used to analyze the molecular structure of supported vanadium oxide species.[42−47]

Oyama et al. investigated the oxygen exchange over silica-supported vanadium oxide catalysts with different vanadia loadings that contained mixtures of surface vanadia species

characterized by a vanadyl stretching vibration at 1042 cm^{-1} and segregated crystalline V_2O_5 particles exhibiting the typical V=^{16}O1 mode of bulk V_2O_5 at 997 cm^{-1} by Raman spectroscopy.[48] The silica-supported vanadyl groups were exchanged at 347 °C, whereas the vanadyl groups in the V_2O_5 crystallites were not affected. The analysis was not trivial because the ^{18}O substitution of the silica-supported vanadyl species shifted the original V=^{16}O band at 1042 cm^{-1} to 997 cm^{-1}, the same position as that for the bulk V=^{16}O1 vibrations in the segregated crystalline V_2O_5 particles.

The shift was confirmed in studies of highly dispersed vanadium oxide species supported on zirconia and silica, respectively, investigating catalysts that do not exhibit spectroscopic features of bulk V_2O_5 particles.[42,43] It is, however, problematic to assign the bands of silica-supported vanadium oxide in the range of 1000−1030 cm^{-1} exclusively to vanadium oxide stretching vibrations because of strong coupling of the V−O modes with the modes of Si−O−V interphase bonds,[45] which also complicates the assignment of the bands due to exchange with $^{18}O_2$.[44]

Ono et al. investigated oxygen exchange in the presence of n-butane and propane at 430−520 °C on ill-defined V_2O_5/SiO_2 catalysts that exhibited a Raman spectrum, which was entirely dominated by segregated V_2O_5 crystallites.[49,50] The bands of V_2O_5 at 998 and 703 cm^{-1} were shifted to 964 and 685 cm^{-1}, respectively, upon dosing of $^{18}O_2$. Oxygen atoms at the V−O3 site (703 cm^{-1}) were found to exchange easier than that at the V=O1 site (998 cm^{-1}) in the presence of n-butane, while in the presence of propane, exchange at the V=O1 site was easier. The difference was ascribed to differences in crystal orientation, lacking any convincing evidence due to the ill-defined, polycrystalline structure of the catalysts.

Taking all this together, it can be said that Raman spectroscopic studies of oxygen exchange on vanadium pentoxide have so far only been carried out on heterogeneous systems. A clear assignment of the Raman bands was therefore not possible. Thus, the changes in the spectra caused by the oxygen exchange under different conditions were difficult to interpret. This motivated us to investigate crystalline V_2O_5 again in depth with Raman spectroscopy. DFT calculations were used to support the assignment of the Raman modes. The spectral changes resulting from the partial exchange of ^{16}O atoms on the surface and in the bulk of V_2O_5 with $^{18}O_2$ from the gas phase at different temperatures and in the presence of different gas atmospheres could thus be clearly elucidated. These studies are model investigations for processes on vanadium-containing mixed metal oxides, which are known for their high performance in alkane and electrocatalytic water oxidation.[51−53] The work contributes to a better understanding of oxygen activation and exchange on vanadium pentoxide, which is important for targeted design with respect to surface or bulk properties of oxidation catalysts. In addition, the study provides reference experiments for *operando* investigations of vanadium oxide-based catalysts.

2. METHODS

2.1. Properties of V_2O_5. According to X-ray diffraction (XRD) (Figure S1 in the Supporting Information and Table S1) and X-ray fluorescence spectroscopy (XRF) analysis, the studied V_2O_5 (internal ID: 22055) was phase pure (orthorhombic phase, space group *Pmmn* (No. 59), point group D_{2h}, ICSD 60767; for lattice parameters, see Table S1), contained no impurities, and it had a specific surface area of 4.2

m^2/g. V_2O_5 was thermally stable under Ar up to 669 °C followed by melting as indicated by an endothermic peak (Figure S2). Melting was accompanied by mass loss due to the evolution of oxygen and sublimation. STEM images (Figure S3) revealed a rod-like shape of the V_2O_5 particles with a size ranging from several hundred nanometers to 3 μm.

2.2. Basic Characterization of V_2O_5. The XRD measurements were performed in Bragg−Brentano geometry on a Bruker AXS D8 Advance II θ/θ diffractometer, using Ni-filtered Cu Kα_{1+2} radiation and a position sensitive energy dispersive LynxEye silicon strip detector. X-ray fluorescence spectroscopy (XRF) was used for elemental analysis of V_2O_5, applying a Bruker S4 Pioneer X-ray spectrometer. For sample preparation, the mixture of V_2O_5 (0.1 g) and lithium tetraborate (8.9 g, >99.995%, Aldrich) was fused into a disk using an automated fusion machine (Vulcan 2MA, Fluxana). Nitrogen adsorption was performed at −196 °C using the Autosorb-6B analyzer (Quantachrome) after outgassing the material in vacuum for 2 h at 200 °C with an external preparation unit (Autosorb Degasser). All data treatments were performed using the Quantachrome Autosorb software package ASWin. The specific surface area S_{BET} was calculated according to the multipoint BET method in the p/p_o = 0.05−0.15 pressure range assuming an N_2 cross sectional area of 16.2 Å^2. Thermogravimetry (TG) and differential thermal analysis (DTA) were carried out on a Netzsch STA449 Jupiter thermanalyzer in 70 N mL/min Ar total flow applying a heating rate of 10 °C/min. Around 80 mg of the sample was placed into the corundum crucible (0.2 mL) without lid. The gas phase analysis during heating was monitored with a quadrupole mass spectrometer (Pfeiffer, QMS200 Thermostar). Evolution of O_2 was recorded by monitoring the change of intensity of the ion currents (m/z = 32). The high angle annular dark field scanning transmission electron microscopy (HAADF-STEM) images were taken on an aberration-corrected JEOL JEM-ARM200F transmission electron microscope operated at 200 kV. The UV/vis spectrum of V_2O_5 was measured using a Cary 5000 UV−vis spectrometer (Agilent) equipped with a Praying Mantis diffuse reflection accessory (Harrick). The data were obtained in percent reflectance and then converted to the Kubelka−Munk function $F(R)$. Spectralon was used as a white standard in the range between 800 and 250 nm.

2.3. Raman Spectroscopy. In a typical Raman measurement, polycrystalline V_2O_5 was either compressed on a glass slide for *ex situ* measurements or placed in the sample holder of a Linkam CCR1000 reaction cell (Linkam Scientific Instruments LTD), or a high temperature reaction chamber from Harrick Scientific Products Inc., respectively, for *in situ* measurements. Except for the experiments presented in Figure 7 using the Harrick Raman chamber, all the *in situ* measurements were conducted in the Linkam cell. The spectra were measured using a customized multiwavelength Raman spectroscopy system (Figure S4) assembled by S&I Spectroscopy & Imaging GmbH (Warstein, Germany). Nine different lasers (785, 633, 532, 488, 457, 442, 355, 325, and 266 nm) were used as excitation sources. Laser powers were tuned by neutral density filters (785 nm, 0.3 mW; 633 nm, 0.2 mW; 532 and 488 nm, 0.5 mW; 266 nm, 0.3 mW; all other lasers, 0.4 mW) to prohibit sample damage. Exposure times (a few seconds to 600 s) were optimized accordingly with regard to a high signal-to-noise ratio. We were aware that V_2O_5 is sensitive to UV lasers (325 and 266 nm), and long exposure times with
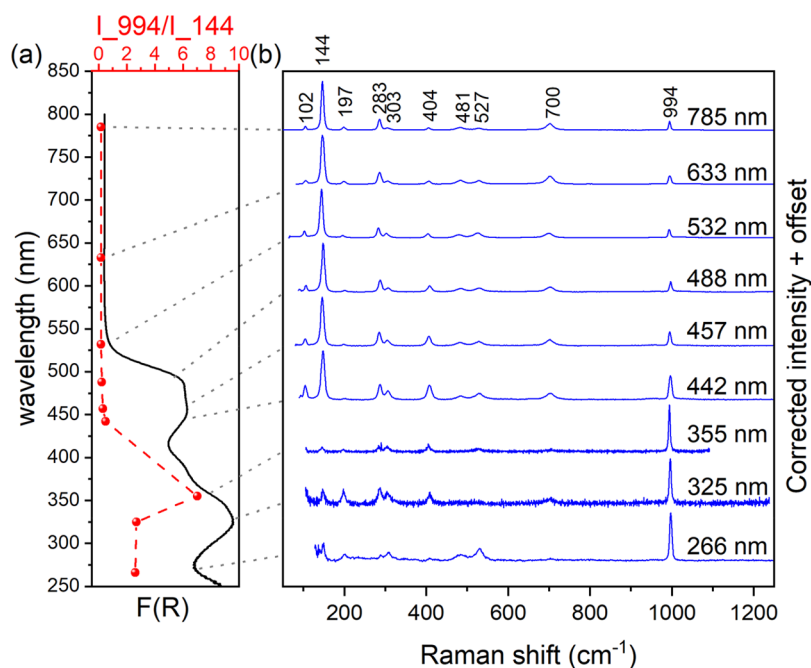
Figure 2. UV/vis spectrum (a) and Raman spectra (b) of V_2O_5 collected at room temperature (*ex situ*). The laser wavelength used for the Raman measurements is shown next to the Raman spectra. The Raman spectra were corrected with respect to instrumental effects, taking into account the known response curve of a white lamp and the absorption spectrum of V_2O_5 (see Figure S8 for details of the correction procedure and Figure S10 for uncorrected spectra); All spectra were normalized to the corresponding maximum band intensity ([0,1]), which differs for the different excitation energies; The band positions indicated were determined for the spectrum measured with the excitation wavelength 532 nm; The intensity ratio of the band at 994 cm^{-1} to the band at 144 cm^{-1} as a function of excitation wavelength is plotted in part a.

relative high laser power could lead to progressive appearance of Raman features around 758, 896, 910, and 1009 cm^{-1} (Figure S5). The laser-induced damage is relevant to structural change due to the removal of vanadyl oxygen as evidenced by the disappearance of the Raman band at 994 cm^{-1}. The entrance slit was set to 100 μm for all measurements. The scattered light was dispersed on 300, 600, or 2400 grooves/mm gratings depending on laser wavelength and resolution requirements, and finally collected by one of the two liquid-nitrogen-cooled CCD detectors (PyLoN:2K and PyLoN:100 from Princeton Instruments). The primary beam was eliminated by using corresponding edge filters. To compare Raman spectra measured by using different excitation lasers, the true Raman scattering intensities were extracted by correcting instrument effects and optical absorption properties of V_2O_5. A standard lamp (deuterium and halogen light source, Ocean Optics DH-2000) with a known emission spectrum was used to correct instrument effects (objectives, filters, gratings, detectors, etc.). In addition, the absorption of light by V_2O_5 was taken into account by the $G(R)$ function that can be calculated from the measured diffuse reflectance spectrum of V_2O_5.[54] A detailed description of the Raman spectroscopy setup and the intensity correction is given in the Supporting Information (Figures S4 and S6−S8).

2.4. Oxygen Isotope Exchange. A 20−50 mg V_2O_5 sample was placed in the Linkam CCR1000 reaction cell unless otherwise mentioned and pretreated by heating the sample at a heating rate of 5 °C/min to the desired temperature under a flow of 20% $^{16}O_2$ (99.999%) balanced by helium (or nitrogen) with a total flow rate of 10 mL/min. Then $^{16}O_2$ was switched to $^{18}O_2$ (97 at% enrichment from the supplier, Linde) to conduct oxygen exchange for 2 h. The fractions of $^{16}O^{16}O$ and $^{16}O^{18}O$, respectively, that were present

as impurities in the $^{18}O_2$ gas cylinder were determined by mass spectrometry and were 1.2% and 2.3%, respectively (Figure S9). Other gases used were propane (Westfalen AG, 99.95%), deuterium labeled propane (Sigma-Aldrich, 99 atom % D), ethane (Westfalen AG, 99.95%), and *n*-butane (Westfalen AG, 99.95%). Raman spectra were measured continuously throughout the exchange process with each spectrum taking 6 or 8 min (532 nm). There is a second thermocouple inserted into the catalyst bed in the Linkam CCR1000 reaction cell to measure the actual temperature. For the Harrick Raman chamber, the heating element and the thermocouple are separated from the reaction part, and thus a calibrated temperature was given.

2.5. Operando Raman Spectroscopy. A 20 mg V_2O_5 sample was placed in the Linkam CCR1000 reaction cell to perform the operando Raman experiments. V_2O_5 was first heated from room temperature to 420 °C at a heating rate of 5 °C/min under 20% $^{16}O_2$ balanced by helium with a total flow rate of 10 mL/min. After reaching 420 °C, the sample was further heated under various reaction feeds ($C_3H_8/^{16}O_2/He$). The effluent gas was connected to a micro-GC (Agilent 490) to perform online gas product analysis. A combination of MS5A (10 m length) and PPQ columns (10 m length), connected to a thermal conductivity detector (TCD), was used to analyze the oxidation products in the gas phase. The conversion of propane X and the product selectivity S were calculated based on the sum of the detected products. Raman measurements were performed simultaneously by using the 532 nm laser during propane oxidation over V_2O_5.

2.6. DFT Calculations. Phonon calculations were performed using Quantum Espresso 5.4.0[55] to obtain vibrational frequencies. The crystal structure of V_2O_5 (Figure 1, 9012221.cif[56]) was obtained from the Crystallography Open Database (COD, Web site: http://www.crystallography.net/

Table 1. Experimentally Determined (Excitation Wavelength 532 nm) Peaks, Calculated Raman Active Phonon Modes (Unit: cm⁻¹), and Vibrational Assignment

mode	exptl[a]	calcd[b] $V_2{}^{16}O_5$ $^{16}O1-^{16}O2-^{16}O3$	calcd[c]	calcd[b] $V_2{}^{16/18}O_5$ $^{18}O1-^{16}O2-^{16}O3$	calcd[b] $V_2{}^{18}O_5$ $^{18}O1-^{18}O2-^{18}O3$	assignment
A_g	102	96.6	107.7	94.7	93.0	T_z translation
	197	192.3	192.8	184.7	181.2	skeleton bending
	303	303.8	294.1	297.4	286.5	R_x libration
	404	400.8	381.7	396.9	383.6	skeleton bending
	481	467.3	527.8	466.3	447.2	O2−V−O3 bending
	527	526.1	542.5	525.4	512.0	O2−V−O3 bending
	994	998.1	1028.9	955.0	955.0	V=O1 stretching
B_{1g}	144	142.5	167.3	138.6	138.4	R_z libration
	283	280.6	276.7	270.7	270.5	O1−V−O3 bending
	700	691.9	772.3	691.0	653.0	V−O3 stretching
B_{2g}	144	133.7	146.0	131.4	129.4	R_y libration
	197	191.8	199.8	184.9	183.1	T_x translation, R_y libration
	303	307.1	298.8	299.5	291.3	R_y libration
	356	350.7	361.3	346.2	340.1	skeleton bending
	481	482.4	528.7	480.7	454.4	displacement of O3
	n.d.[d]	944.7	1010.3	935.6	900.7	V−O2 stretching
	994	997.6	1030.1	964.2	953.4	O1−V−O2 stretching
B_{3g}	144	144.4	168.7	140.5	140.2	T_y translation
	n.d.	214.2	218.6	214.9	203.0	R_x libration
	283	281.9	279.0	272.4	271.6	O1−V−O2 bending
	700	691.5	772.4	690.5	652.6	V−O3 stretching

[a]Experimental Raman spectra are shown in Figure 2b, the peak positions were determined using the 532 nm laser. [b]Calculated Raman active phonon modes, this work [c]Calculated Raman active phonon modes from reference.[66] [d]n.d.: not detected.

cod/index.php), which was used as the initial input structure. The structure was optimized by variable cell relaxation calculations (Tables S1 and S2). The calculations were carried out by using the Perdew−Burke−Ernzerhof (PBE) functional and ultrasoft pseudopotentials. A van der Waals-inclusive correction (DFT-D)[57,58] was applied to take dispersion forces between layers into account. The plane wave kinetic energy cut off values of 60 and 480 Ry were adopted for V_2O_5 for the wave functions and the charge densities, respectively. A Methfessel−Paxton smearing of 0.01 Ry was used to improve calculation performance. Here, $6 \times 6 \times 6$ Monkhorst−Pack grids of k-point sampling was chosen for V_2O_5.[59]

3. RESULTS AND DISCUSSION

3.1. Experimental and Calculated Raman Spectra of V_2O_5. Generally, the Raman spectrum of V_2O_5 can be divided into (i) the high energy range from 1000 to 500 cm⁻¹ where V−O stretching vibrations arise, (ii) the medium energy range from 500 to 300 cm⁻¹ where V−O−V bending vibrations arise, and (iii) the low energy range $\nu \sim <300$ cm⁻¹ where collective vibrations of $(V_2O_5)_n$ units arise. Based on the symmetry of the crystal structure (space group $Pmmn$ (No. 59), point group D_{2h}), analysis using the Bilbao crystallographic server (Web site: http://www.cryst.ehu.es/) results in 39 optical modes

$$\Gamma_{optic} = 7A_g + 3A_u + 3B_{1g} + 6B_{1u} + 7B_{2g} + 3B_{2u} + 4B_{3g} + 6B_{3u}$$

in which 21 modes are Raman active

$$\Gamma_{Raman} = 7A_g + 3B_{1g} + 7B_{2g} + 4B_{3g}$$

According to the light absorption properties of V_2O_5 in the UV/vis range (Figure 2a), the experimental Raman spectra of V_2O_5 recorded using nine different lasers can be grouped into off-resonance Raman spectra (785 and 633 nm), one preresonance Raman spectrum (532 nm), and resonance Raman spectra (488 to 266 nm). As shown in Figure 2b, 10 distinct bands were resolved experimentally. Note that the band at 102 cm⁻¹ is not observed with the UV lasers (266, 325, and 355 nm) due to cutting off by the edge filter. The excitation wavelength has no significant effect on the band position. The peak maximum at 1001.4 ± 0.54 cm⁻¹ of the standard polystyrene was deviating by less than 3 cm⁻¹ with all lasers (Figure S7). Raman shifts indicated in Figure 2b were determined based on the spectrum of V_2O_5 measured with the 532 nm laser. In addition, six weak bands were observed at 1025, 962, 800, 660, 356, and 232 cm⁻¹ with the 785 nm laser (Figure S10, parts b and c).

With the increase of photon energy (decrease of excitation wavelength), the intensity ratio of the band at 994 cm⁻¹ to the band at 144 cm⁻¹ increases and exhibits a maximum at 355 nm (Figure 2a) suggesting resonance enhancement of the band at 994 cm⁻¹ by using excitation energies in the UV range.[60] However, the probing depths changes with the excitation wavelength as well. Therefore, the change in the intensity ratio may also reflect structural gradients within the depth profile. UV lasers are more surface sensitive.[61] Consequently, the relative low intensities of bands at lower wavenumbers in the spectra recorded with the UV lasers, which are due to long-range order, can be interpreted in terms of restructuring and formation of a near surface region, which exhibits less long-range order.

Various experimental and theoretical studies contributed to an assignment of the peaks observed in the Raman spectrum of V_2O_5.[62−66] However, some inconsistencies occur in the literature. Therefore, phonon calculations were performed to refine the assignment. The calculated lattice parameters of the optimized structure agree very well with the lattice parameters of the investigated V_2O_5 material determined by XRD (Table S1), indicating that the model represents reality quite well. The

atomic coordinates of the optimized calculated V_2O_5 structure are given in Table S2. Experimentally determined peaks measured by using the 532 nm laser are compared with calculation results of the present and a previous study[66] in Table 1 and Figure S11. In Figure S11, the atomic displacement patterns of all calculated Raman active phonon modes are shown. The peak positions calculated in the present work agree well with the experiment. The largest deviation is 14 cm^{-1}. However, not all calculated modes are resolved experimentally (resolution ~0.5 to ~7 cm^{-1}, please see Figure S6). Each of the six bands found at 197, 283, 303, 481, 700, and 994 cm^{-1} is caused by two different calculated modes (Table 1). The most pronounced band at 144 cm^{-1} is composed of three different modes calculated at 133.7, 142.5, and 144.4 cm^{-1}. Two modes calculated at 214.2 and 944.7 cm^{-1} were not observed experimentally, most likely due to low Raman intensity.

Table 1 provides the assignment of all experimental modes according to the present DFT calculations. The band at 994 cm^{-1} is frequently exclusively attributed to the V=O1 stretching mode.[65] Our results show that the 994 cm^{-1} band has noticeable contribution from O1−V−O2 stretching, hence, it involves O1 and O2 atoms.

The band observed at 527 cm^{-1} was assigned to V−O2−V symmetric stretching by Abello et al.[63] In contrast, the same band was attributed to V−O3 bond stretching and V−O3−V angle deformation by Clauws et al.[64] and Brázdová et al.[65] Based on the present calculations (Table 1), the mode involves both O2 and O3, and it is related to O2−V−O3 bending, which is in agreement with Zhou et al.[66]

Major inconsistencies exist concerning the involvement of the three different oxygen atoms in the V_2O_5 structure to the bands observed at 404 and 481 cm^{-1}, which were ascribed to O2 and O3 atoms displacements, respectively, by Abello et al.[63] Clauws et al., however, ascribed the bands to O1 and O2 atoms displacements, respectively.[64] In turn, Brázdová et al. proposed the two bands to O3 and O2 atom displacement, respectively.[65] Here we assign the band at 404 cm^{-1} to skeleton bending involving all three oxygen atoms and the vanadium atom (Table 1). The band at 481 cm^{-1} originates from O2−V−O3 bending and the displacement of the O3 atom (Table 1).

The four weak and broad bands located at around 1025, 962, 800, and 660 cm^{-1}, which were clearly observed by using the infrared laser (785 nm) (Figure S10b), have been tentatively assigned to overtones or combination bands in previous studies.[63,64] In contrast, Brázdová et al.[65] assigned the band at 962 cm^{-1} to a fundamental band (V−O2−V stretching, B_{2g} mode). A band ascribed to V−O2 stretching was predicted at 944.7 cm^{-1} in our study (Table 1), which, however, deviates considerably from the experimentally observed band at 962 cm^{-1}. The band at around 1025 cm^{-1} may arise from surface VO$_x$ species self-supported on V_2O_5, because VO$_x$ species supported on oxides similarly exhibit a broad feature in the range between 1012 and 1027 cm^{-1}.[67] The assignment of the band observed at 232 cm^{-1} with the 785 nm laser excitation (Figure S10c) remains unclear so far. The closest calculated value of 214.2 cm^{-1} is due to a collective vibration of the V_2O_5 lattice.

The assignment of the bands is an important prerequisite for the interpretation of the shift of bands observed during isotope exchange.

3.2. Oxygen Isotope Exchange. Isotope exchange of oxygen on the surface and in the bulk of polycrystalline $V_2{}^{16}O_5$ with $^{18}O_2$ in the gas phase was studied by Raman spectroscopy at different temperatures and chemical potentials. The temperatures of ca. 320, 430, and 570 °C applied in the present study were chosen below, at and above typical reaction temperatures in selective oxidation of alkanes over vanadium oxide based catalysts, respectively. All temperatures are distinctly above the Tammann temperature $T_{Tam}(V_2O_5)$ of 204 °C (477 K). At the Tammann temperature, $T_{Tam} \approx 0.5 T_{melt}$ [K], atoms or ions become sufficiently mobile and migration from the bulk to the surface and surface liquefaction are possible. The exchange was probed in synthetic air and in the presence of alkanes and the type of oxygen atom exchanged was concluded based on the results of the DFT calculations.

3.2.1. Prediction of Raman Shifts in Partially and Fully Exchanged V_2O_5 by DFT Calculations. The changes in the Raman spectrum of V_2O_5 were predicted by DFT calculations for two cases:

(i) only ^{16}O1 is exchanged by ^{18}O
(ii) all three types of oxygen atoms are exchanged by ^{18}O

The calculated peak positions for the two cases are listed in Table 1.

(i) The exchange of the O1 atom will have an impact on the position of the experimentally determined band at 994 cm^{-1}, which contains contributions of two different phonon modes as explained above. The A_g mode is related to O1 (V=O1 stretching) and the B_{2g} mode is related to O1 (major contribution) and O2 atoms (minor contribution) in an O1−V−O2 stretching vibration (Table 1). The calculated values of A_g at 998.1 cm^{-1} and B_{2g} at 997.6 cm^{-1} in $V_2{}^{16}O_5$ differ slightly and are experimentally not resolved, giving rise to only one experimentally observed band at 994 cm^{-1} in $V_2{}^{16}O_5$. However, when ^{16}O atoms are exchanged by ^{18}O only at the V=O1 site, the calculated A_g and B_{2g} modes shift differently by 43.1 cm^{-1} to 955.0 cm^{-1} and by 33.4 cm^{-1} to 964.2 cm^{-1}, respectively (Table 1). Hence, the appearance of two new peaks at lower energy is expected. It should be possible to resolve these peaks experimentally due to the difference of about 10 cm^{-1}. In addition, the O1 atom contributes to the B_{1g} mode with an O1−V−O3 bending vibration (calculated shift at 280.6 cm^{-1}) and to the B_{3g} mode with an O1−V−O2 bending vibration (calculated shift at 281.9 cm^{-1}). The two modes are giving rise to the experimentally observed band of $V_2{}^{16}O_5$ at 283 cm^{-1} (Table 1). The calculated Raman shifts are moved by 9.9 and 9.5 cm^{-1}, respectively, to 270.7 and 272.4 cm^{-1}, respectively, when just the O1 atom is exchanged. Hence, it is expected that this band will not split into two components in the experimental spectrum and will shift only slightly to lower energy. In particular, when the oxygen exchange is not complete, the shift will be negligible.

(ii) When all types of oxygen atoms are exchanged to ^{18}O, all bands are shifted to lower energies and are different from case i. A_g and B_{2g} modes (994 cm^{-1}) shift in a similar manner by ca. 44 cm^{-1} to 955.0 and 953.4 cm^{-1}, respectively.

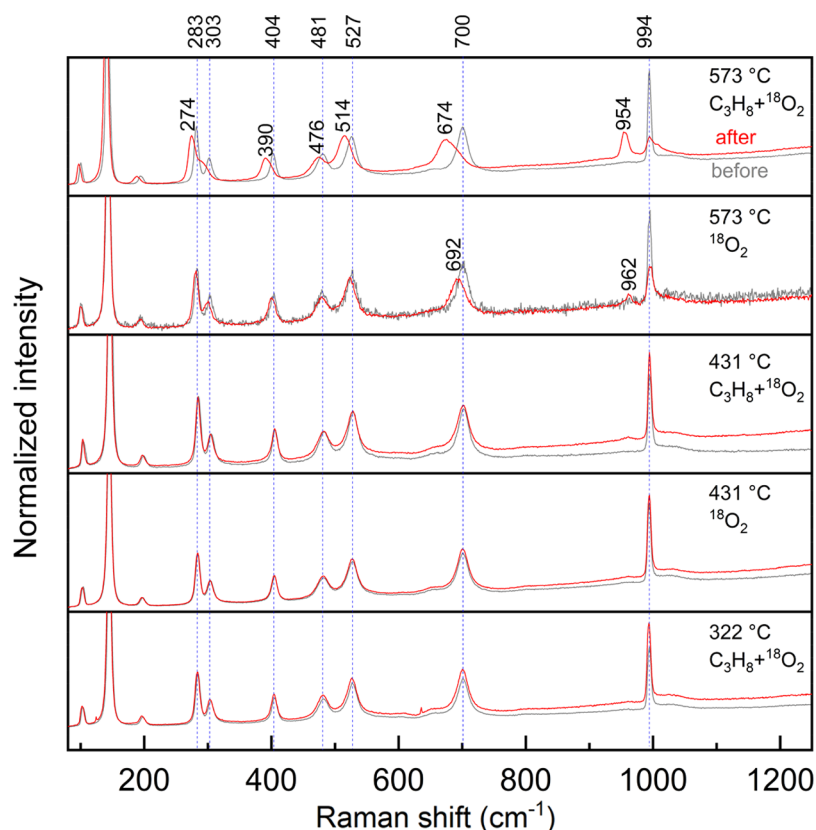*3.2.2. Experimentally Observed Changes in the Raman Spectra. 3.2.2.1. Temperature Effect in the Presence of*

Figure 3. Raman spectra of V_2O_5 measured at room temperature before and after isotopic oxygen exchange; Gray and red spectra denote the cases before and after exchange at 322, 431, and 573 °C, respectively, using $^{18}O_2$ (20% in He) or a mixture of propane and oxygen (C_3H_8 (1%) + $^{18}O_2$ (19%) in He) for 2 h. All the spectra were normalized to [0,1]. The positions of all spectra were aligned with respect to the band at 994 cm^{-1}. Laser: 532 nm. Heating rate: 5 °C/min. Total flow rate: 10 mL/min.

Oxygen Only. No change in the Raman spectrum was detectable when a flow of 20% $^{16}O_2$ in helium was exchanged by a flow of 20% $^{18}O_2$ in helium at 431 °C (Figure 3).

At 573 °C, however, the peak at 994 cm^{-1} lost intensity. Taking into account the results of the DFT calculations of partially (O1) and fully (O1, O2, O3) exchanged V_2O_5, the Raman spectra recorded at room temperature after the isotope exchange experiments at different temperatures were deconvoluted to get insight into the contributing components in a qualitative manner (Figure 4). The deconvolution procedure is explained in detail the Supporting Information. The fitting parameters are provided in Table S3.

Figure 4a, middle, shows the V−O3 stretching vibrations, whereas Figure 4b, middle, shows V=O1 and O1−V−O2 stretching vibrations after exchange in 20% $^{18}O_2$ in helium at 573 °C. Two components at higher energy (features >1000 cm^{-1} assigned above to surface VO_x species) become visible now at 1007 and 1029 cm^{-1}, which might be attributed to V=$^{18}O_{(s)}$ and V=$^{16}O_{(s)}$, respectively (Figure 4b, middle). The two components appear also after exchange in the presence of propane (see Section 3.2.2.2 and Figure 4b, top). Interestingly, the peak width of V=$^{16}O_{(s)}$ species in terms of fwhm (full width at half-maximum) is much larger than that of V=$^{18}O_{(s)}$ (∼50 vs ∼15 cm^{-1}, Table S3). The large peak width in the spectrum before oxygen exchange reflects the heterogeneity of the VO_x species at the surface. This may mean that the reactivity of the energetically different surface species is also different. The relatively small peak width of V=$^{18}O_{(s)}$ suggests that only a portion of the V=$^{16}O_{(s)}$ species

is reactive and has been exchanged. Assuming an isotope ratio of 1.0452, one would expect a band at ∼1050 cm^{-1} for this reactive V=$^{16}O_{(s)}$ species. The exposure of the V_2O_5 to C_3H_8 + $^{16}O_2$ feed alone does not cause any spectral modification (Figure S12), suggesting that the observed change in the presence of oxygen at high temperature is indeed due to a partial oxygen exchange and not, for example, due to the formation of defects.

In addition, a new band appeared at around 962 cm^{-1} ($^{18}O1$−V−$^{16}O2$) with a shoulder around 954 cm^{-1} (V=$^{18}O1$) (Figure 4b, middle). The deconvolution of the original spectra is shown in the Supporting Information, Figure S13. The band at 702 cm^{-1} moved to 690 cm^{-1}, suggesting a partial exchange of the O3 atom, which affects the V−O3 stretching vibration (Figure 4a, middle). Shifts of bands below 530 cm^{-1} are hardly visible. The observations suggest that oxygen atoms at the V=O1 and V−O3 sites were partially exchanged in the presence of 20% $^{18}O_2$/He at 573 °C.

The temporal evolution of spectra recorded *in situ* during the experiment at 573 °C is shown in Figure 5a. The gradual increase of the new band around 962 cm^{-1} is clearly observed reflecting the increase of the exchange extent. The band positions of original bands are not affected, showing that the extent of exchange (O1 atoms) has no influence on the band position.

3.2.2.2. Oxygen Isotope Exchange in the Presence of Propane. The following experiment explores how the chemical potential of the gas phase influences the oxygen exchange at different temperatures. For this purpose, propane was added to
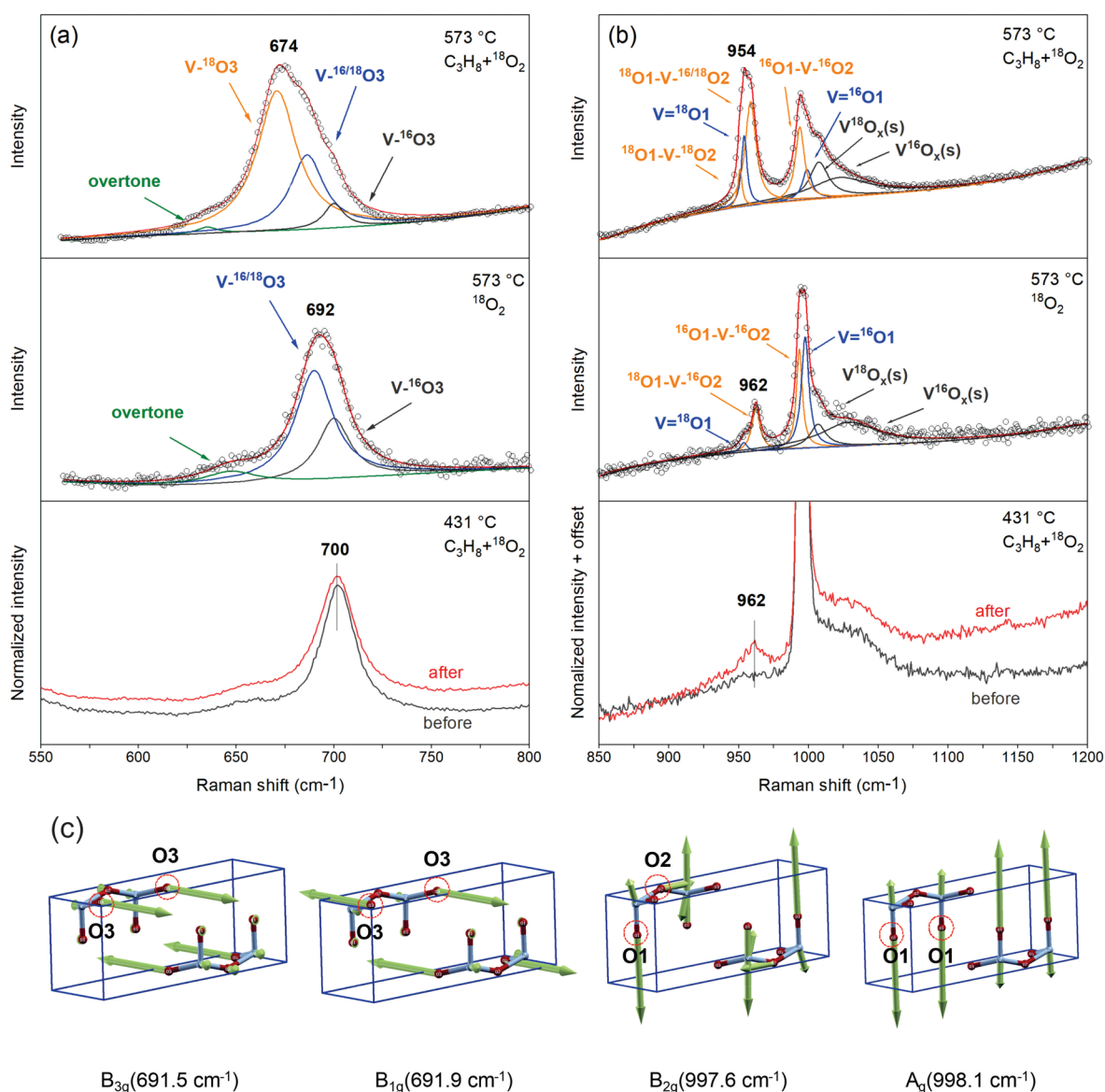
Figure 4. Deconvolution of Raman spectra collected at room temperature after treatment at different temperatures and in different gas atmospheres (the same Raman spectra as shown in Figure 3) in the V−O3 (a) as well as V=O1 and O1−V−O2 stretching vibration region (b). Temperatures and gas atmospheres are specified in the right top corner of each section. (c) Corresponding representations of vibrational motions of phonon modes.

the oxygen flow. The presence of propane, which undergoes oxidation under the applied conditions (propane conversion X = 36% at 573 °C), will change the defect concentration on the surface and in the bulk of the vanadia. A low ratio of propane to oxygen (1:19) was used to prevent severe reduction of V_2O_5, in particular at the high reaction temperatures.

When a flow of C_3H_8:$^{18}O_2$:He in a ratio of 1:19:80 was applied at 573 °C, the intensity of the band at 994 cm^{-1} decreased significantly and all other bands moved to lower wavenumbers (Figures 3, 4a, 4b(top), and 5b). A new band appeared at around 954 cm^{-1}. This is different from the case using 20% $^{18}O_2$ in helium (Figures 4a, 4b(middle), and 5a), where the development of a band at 962 cm^{-1} with a shoulder around 955 cm^{-1} was observed. Specifically, the extent of exchange of O3 atoms is higher than under only oxygen flow as indicated by the larger shift of the position of the peak near 700 cm^{-1} and the appearance of a component of full V−$^{18}O3$ in this band (Figure 4a(top)). The deconvolution analysis

further reveals that the newly formed band at 954 cm^{-1} possibly contains three components from different combinations of exchanged O1 and O2 atoms due to V−O1 and O1−V−O2 stretching vibrations (Figure 4b(top)). The presence of a component corresponding to $^{18}O1-V-^{16/18}O2$ (coupling of O2 atoms) suggests a faster exchange of O1 atoms with ^{18}O as compared to O2 atoms. Bearing in mind the calculated Raman spectrum of $V_2^{18}O_5$ (Table 1), the results suggest that essentially all three types of oxygen atoms were exchanged in the presence of propane at 573 °C. In a control experiment, $^{16}O_2$ instead of $^{18}O_2$ was used (Figure S12). According to that, propane oxidation at this high reaction temperature does not change the structure of V_2O_5 so drastically as to affect the Raman spectrum. Consequently, the change in band positions presented in Figure 3 is due to ^{18}O incorporation into V_2O_5. These results directly prove that the presence of a reductant accelerates exchange rates.[29,34] Assuming the R2 exchange mechanism over V_2O_5, two surface vacancies are required to
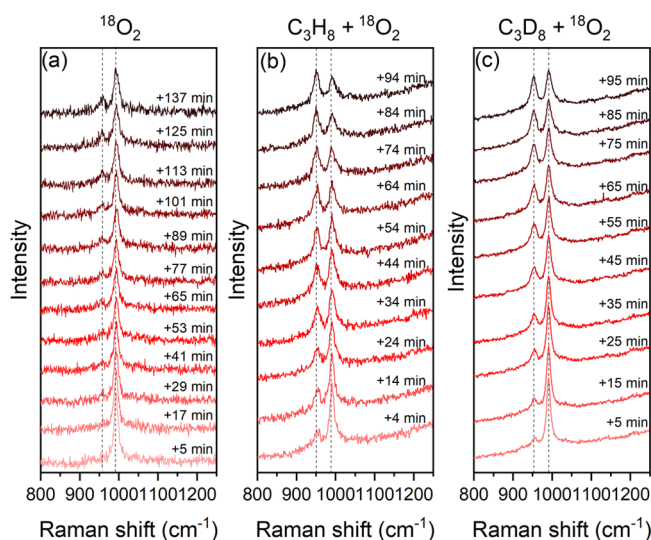
Figure 5. *In situ* Raman spectra of V_2O_5 at 573 °C under 20% $^{18}O_2$ in He (a), 1% C_3H_8 + 19% $^{18}O_2$ in He (b), and 1% C_3D_8 + 19% $^{18}O_2$ in He (c) as a function of time. Conditions of exchange experiments are described in the caption of Figure 3. The numbers show the time that had passed since the start of the experiment at the moment of recording. Laser: 532 nm.
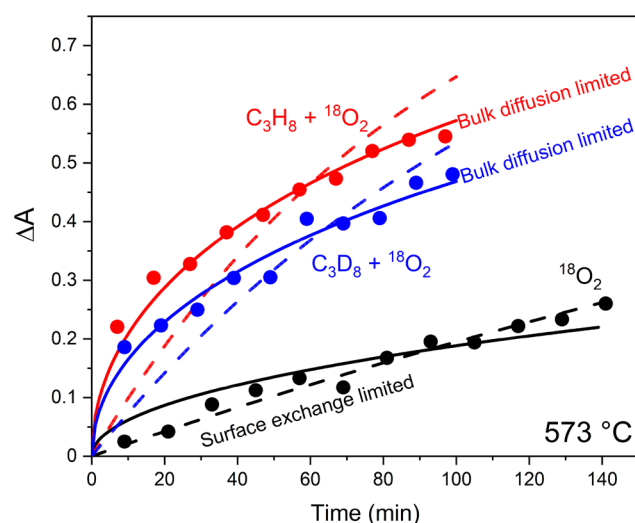

Figure 6. Extent of oxygen exchange as a function of time; The lines are the fitted results using eqs 3 (dashed) and 4 (solid). The experimental data points were taken from the experiments shown in Figure 5. Note that the time used in the graph is the average time taken to record each spectrum.

make exchange happen.[28] It is likely that propane effectively generates vacancies on the surface of V_2O_5 and greatly increases the probability of having two neighboring vacancies. DFT calculations also imply that reduced surfaces of metal oxides are energetically more favorable for oxygen activation than unreduced surfaces.[40] It was pointed out that the formation energy of surface oxygen vacancies is reduced by the presence of surface OH groups due to a weakening of the V−O bond in V−OH.[68] To verify this, deuterium labeled propane was used in the isotopic oxygen exchange experiment. The exchange proceeds indeed at a slightly lower rate in the case of using deuterium labeled propane as compared to normal propane (Figure 5c). The exchange extent at each time step is lower than that using normal propane. The observed isotope effect suggests that hydrogen is involved in the oxygen activation process, possibly by reducing the energy to form oxygen vacancies at the surface.

To further quantify the exchange process, the exchange extent ΔA,

$$\Delta A = \frac{A_{new}}{A_{new} + A_{994}} \tag{2}$$

where A refers to the band area, as a function of time (Figure 5) was analyzed at 573 °C in the different gas atmospheres (Figure 6). The analysis does not allow the differentiation between the three types of oxygen atoms. Instead, the total extent of exchange is estimated. In general, isotopic oxygen exchange comprises surface exchange and bulk diffusion.[69−71] Surface exchange takes place at the interface between the solid and the gas. The propane molecule would also be involved in the surface exchange by reacting with labeled surface oxygen species and generating oxygen vacancies. Bulk diffusion of oxygen can proceed through vacancies or interstitial sites.[72] In the following, the two borderline cases

$$\Delta A = 1 - \exp\left(-\frac{3k_{ex}t}{a}\right) \quad \text{surface exchange limited} \tag{3}$$

and

$$\Delta A = 1 - \sum_{n=1}^{\infty} \left[\frac{6}{(n\pi)^2} \exp\left(-\frac{(n\pi)^2 Dt}{a^2}\right) \right]$$

bulk diffusion limited   (4)

where k_{ex} refers to the surface oxygen exchange coefficient, D is the oxygen diffusion coefficient, and a is the radius of the spherical catalyst particles, have been considered. The assumption of spherical particles is a rather crude simplification in view of the plate-like nature of the V_2O_5 particles (Figure S3). However, a comparison of relative changes is possible. The detailed derivation of eqs 3 and 4 and the fitting parameters (Table S4) are provided in the Supporting Information. As Figure 6 shows, oxygen exchange at 573 °C remains limited to the surface in the absence of propane (Figure 6, black lines and data points). Studies of oxygen exchange on amorphous V_2O_5 at 400−550 °C have shown that, in the absence of a reducing agent, the rate of exchange is controlled by the surface reaction.[73] In the presence of propane, however, the overall exchange rate appears to be limited by the bulk diffusion (Figure 6, red and blue lines and data points). Apparently, propane at 573 °C accelerates oxygen exchange at the surface, so that oxygen diffusion in the bulk becomes a comparatively slow process.

The main bands positions were not shifted when the same experiment was performed at 431 °C (Figures 3 4a, and 4b(bottom)). The temperature 431 °C is a typical reaction temperature applied in alkane oxidation over V-based catalysts. Just a small intensity difference near 962 cm^{-1} was found indicating that the oxygen exchange is just detectable by Raman spectroscopy at this temperature and mainly V═O1 sites were exchanged (Figure 4b, bottom). In contrast, oxygen exchange at the same temperature in pure oxygen could not be detected by Raman spectroscopy. Due to the small extent of exchange at 431 °C, it was not possible to perform a kinetic analysis in analogy to the experiment at 573 °C (Figure 6). However, since oxygen diffusion in the bulk is even more
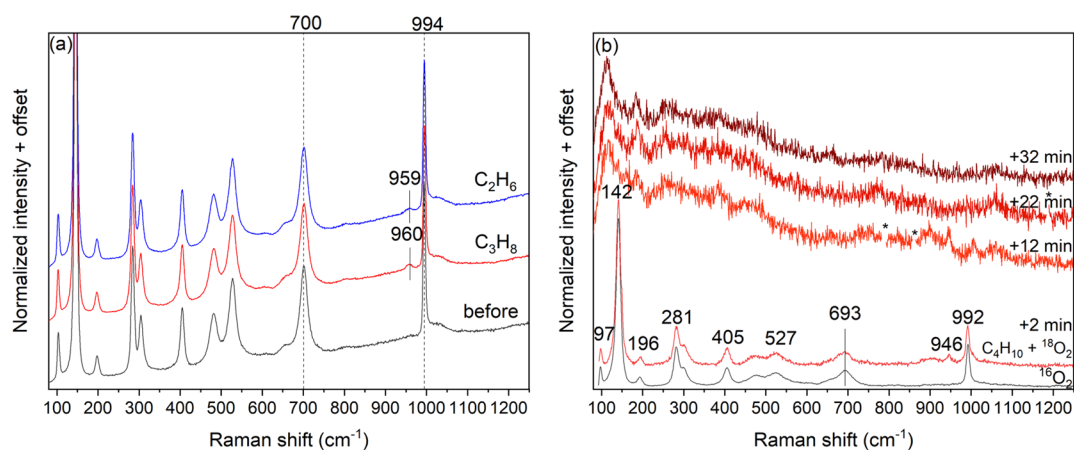
Figure 7. Effect of the nature of the alkane on isotope oxygen exchange. (a) Raman spectra of V_2O_5 measured at room temperature before and after isotopic oxygen exchange experiments under 10% C_3H_8 + 5% $^{18}O_2$ and 10% C_2H_6 + 5% $^{18}O_2$, respectively, at 400 °C. (b) *In situ* Raman spectra of V_2O_5 at 400 °C under $^{16}O_2$ and 10% C_4H_{10} + 5% $^{18}O_2$ as a function of time. Numbers on the spectra indicate the starting time of measurement. Asterisks represent cut cosmic ray signals. Raman spectra were normalized to [0,1]. Laser: 532 nm. Exchange experiments were conducted at 400 °C for 2 h in the Harrick Raman chamber. Heating rate: 5 °C/min. Total flow rate: 10 mL/min.

Table 2. Types of Oxygen Atoms in V_2O_5 Exchanged at Different Temperatures and in Different Gas Atmospheres

	gas phase composition (vol %)			temperature of oxygen exchange (°C)			
	alkane	O_2	inert	573	431	400	322
O_2/He	0	20	80	O1, O3	n.d.[a]	—[b]	—
C_2H_6/O_2	10	5	85	—	—	O1	—
C_3H_8/O_2	1	19	80	O1, O2, O3	O1	—	n.d.
	10	5	85	—	—	O1	—
C_4H_{10}/O_2	10	5	85	—	—	O1, O2[c]	—

[a] n.d.: not detectable by Raman spectroscopy. [b] —: not analyzed. [c] Observation difficult due to superimposed reduction of V_2O_5

difficult at lower temperatures, it is very likely that this process does not play a role in the lower temperature range.

Finally, the exchange in the presence of propane was also performed at 322 °C. No change in the Raman spectrum was observed under these conditions after 2 h (Figure 3).

The direct comparison of the present *in situ* Raman experiments with kinetic studies of isotopic oxygen exchange by mass spectroscopy in the past is not possible, as these experiments were carried out in vacuum at low oxygen partial pressures of a few millibar,[28,29] which were lower than or in the order of the magnitude of the equilibrium oxygen partial pressure that develops above V_2O_5 at elevated temperatures.[74−76] Online mass spectra recorded during a temperature programed experiment in the Raman cell in the presence of 20% $^{18}O_2$ in He show that the onset temperature for observing mixed $^{16}O^{18}O$ in the gas phase was ~424 °C (Figure S9), and for $^{16}O_2$ at ~450 °C, which is in agreement with the observation that no oxygen exchange was observed by Raman spectroscopy at 431 °C in 20% $^{18}O_2$ in He (Figure 3). The Raman spectroscopy appears a little less sensitive than the mass spectroscopy. Furthermore, an increase in the relative concentration of ^{16}O atoms in the gas phase oxygen also occurred at ~424 °C, which confirms that the oxygen exchange between the gas phase and the solid starts at temperatures higher than 420 °C in absence of a reducing agent, because in the case of a full gas-phase R^0 mechanism a constant atomic ratio of ^{16}O would be expected. The formation of $^{16}O^{18}O$ further implies that oxygen dissociation (eq 1) on V_2O_5 is reversible, which is different from a previous work, in which no

formation of $^{16}O^{18}O$ was found from $C_3H_8-^{16}O_2-^{18}O_2$ mixtures on $V^{16}O_x/Zr^{16}O_2$ at about 427 °C.[77]

3.2.2.3. Influence of the Hydrocarbon Chain Length. The effect of the nature of the alkane on the isotope oxygen exchange was examined at 400 °C applying an alkane:oxygen ratio of 10:5. These conditions correspond to the typical temperature and feed composition used in the oxidative dehydrogenation of alkanes. Ethane, propane, and *n*-butane were compared. In case of ethane and propane, a small band near 962 cm^{-1} occurs after 2 h under these conditions, while all the other bands maintain their positions (Figure 7a). Apparently, mainly a small fraction of V=O1 sites was exchanged. By using *n*-butane, a new band at 946 cm^{-1} is already formed after 2 min (Figure 7b). No change in the Raman spectra was observed after such a short time in the experiments with ethane and propane. As compared to the spectrum obtained under $^{16}O_2$ at the same temperature, the band at 700 cm^{-1} (shifted to 693 cm^{-1} due to thermal effect) maintains its position as well as other bands. V_2O_5 was fully reduced, however, after only 12 min, and no clear features can be found in the *in situ* Raman spectra anymore (Figure 7b). The more reducing conditions in *n*-butane lead most likely to a higher concentration of surface oxygen vacancies. The newly formed band at 946 cm^{-1} is attributed either to isotope oxygen exchange (see band at 953.4 cm^{-1} for $^{18}O1-V-^{18}O2$ stretching in Table 1) or to an intermediate (suboxide) during reduction of V_2O_5.

4. GENERAL DISCUSSION AND CONCLUSIONS

V_2O_5 was studied using multiwavelength Raman spectroscopy. Reassignment of the experimentally observed active Raman vibrational modes using DFT calculations revealed that the band at 994 cm^{-1}, which in previous studies was attributed exclusively to the vanadyl oxygen stretching vibration (V=O1), contains additional contributions from O2 atoms. Based on the present combined experimental and theoretical approach, a method was developed to unambiguously determine the nature of the oxygen atom in the crystal structure of V_2O_5 (O1, O2, or O3) exchanging with $^{18}O_2$ in the gas phase. The new assignment makes it possible to determine experimentally which type of oxygen atom can be exchanged under which reaction conditions. The exchange position depends strongly on the temperature and the chemical potential in the gas phase. An overview of the cases studied in the present work is given in Table 2. The conditions investigated are important for the selective and total oxidation of alkanes.

For example, in the presence of propane, but under quite oxidative conditions (1% C_3H_8, 19% O_2), only O1 oxygen atoms are exchanged at 431 °C. This temperature is in the range where selective oxidation reactions of alkanes are typically carried out. Using eq 2, a degree of exchange of ~6.8% is measured by Raman spectroscopy after 2 h under these conditions. Since the probing depth of Raman spectroscopy is limited and ranges between a few and several hundreds of nanometers depending on the energy of the exciting laser, the overall exchange extent of the entire sample is much smaller than this value. The very low degree of exchange, which was only detectable after prolonged reaction time (2 h), indicates that the oxygen isotope exchange occurs mainly at the surface and/or in a near-surface region under the applied conditions. With increasing temperature in an oxidative atmosphere or in the presence of reducing agents, O3 sites and eventually O2 sites are exchanged. All types of oxygen (O1, O2, and O3) are involved in the exchange at very high temperatures (573 °C) and in the presence of propane in the feed. Under these conditions, a kinetic analysis utilizing spectral changes as a function of time was possible. The analysis shows that oxygen vacancies generated by propane facilitate the incorporation of gaseous oxygen into the lattice of V_2O_5 by accelerating the surface exchange process. Hence, rapid oxygen exchange at 573 °C in the presence of propane appears to be limited by bulk diffusion.

The exchange of oxygen in V_2O_5 becomes energetically increasingly difficult in the following order: O1 < O3 < O2. The terminal vanadyl defects are the easiest to form in agreement with predictions by theory.[9,78] Under typical reaction conditions of propane oxidation (400−450 °C), mainly vanadyl oxygen O1 is involved in the oxygen exchange and the very low exchange extent suggests that the exchange occurs primarily on the surface and/or the near surface region. With a classical feed composition ($C_3H_8:O_2$ = 2:1) and temperature (400 °C) of the oxidative dehydrogenation of propane, hardly any change is seen in the spectrum and this small change only affects O1. In this temperature range, the working catalyst in the Raman cell produces propene by oxidative dehydrogenation of propane and CO_2 as the product of total oxidation (Figure S14). The selectivity to propene under these conditions and at low conversions, which are typically set for kinetic studies, is between 55 and 60%. The

catalyst was working in steady-state (Figure S14), and consequently, no changes in the Raman spectra are observed with time on stream. Also under other reaction conditions, no changes were detected after a total reaction time of 7 h (Figure S14).

In vanadium oxide based systems, it is commonly assumed that the formation of propene and other oxidation products occurs according to the Mars−van Krevelen mechanism,[79] which would involve consumption of surface oxygen atoms by incorporation of surface or lattice oxygen into water or oxygen-containing oxidation products. As far as propane oxidation on vanadium oxide catalysts is concerned, these conclusions are mainly based on kinetic modeling,[77,80] or DFT calculations at 0 K.[81] In the present work, the basis for the assignment of the Raman bands of $V_2(^{16}O,^{18}O)_5$ was provided. The isotope exchange experiments presented here cast doubt on whether the Mars−van Krevelen mechanism prevails under typical conditions of selective oxidation of propane, since a very small change in the spectra was observed only after 2 h of operation at 400 °C, indicating some exchanged O1 atoms (Figure 7a), while the catalyst produced propylene and CO_2 at the steady state long before these changes were observed in the Raman spectra (Figure S14a). However, due to the limited sensitivity of Raman spectroscopy, further systematic *operando* investigations in combination with mass spectrometry are needed here to obtain more clarity.

■ ASSOCIATED CONTENT

ⓢ Supporting Information

The Supporting Information is available free of charge at https://pubs.acs.org/doi/10.1021/acs.jpcc.2c00174.

> XRD pattern of V_2O_5, TG and DTA analysis of V_2O_5, HAADF-STEM images of V_2O_5, description of multiwavelength Raman spectroscopy, mass spectra of oxygen exchange of V_2O_5, uncorrected Raman spectra of V_2O_5, the atomic displacement patterns of Raman active phonon modes, Raman spectra of V_2O_5 after treatment in the presence of C_3H_8 and $^{16}O_2$ at 573 °C, table of calculated lattice parameters and bond lengths, table of atomic coordinates of the optimized structure, description of the deconvolution of Raman spectra, discussions of surface reaction and bulk diffusion, and *operando* Raman spectroscopy of V_2O_5 during propane oxidation (PDF)

■ AUTHOR INFORMATION

Corresponding Author

Annette Trunschke − *Fritz-Haber-Institut der Max-Planck-Gesellschaft, D-14195 Berlin, Germany;* ⦿ orcid.org/0000-0003-2869-0181; Email: trunschke@fhi-berlin.mpg.de

Authors

Yuanqing Wang − *Fritz-Haber-Institut der Max-Planck-Gesellschaft, D-14195 Berlin, Germany; BasCat, UniCat BASF Jointlab, Technische Universität Berlin, D-10623 Berlin, Germany;* Present Address: Materials Genome Institute, Shanghai University, 200444, Shanghai, China; ⦿ orcid.org/0000-0002-1332-7956

Frank Rosowski − *BasCat, UniCat BASF Jointlab, Technische Universität Berlin, D-10623 Berlin, Germany; Heterogeneous Catalysis, BASF SE, Process Research and Chemical Engineering, D-67065 Ludwigshafen, Germany*

Robert Schlögl − *Fritz-Haber-Institut der Max-Planck-Gesellschaft, D-14195 Berlin, Germany; Max-Planck-Institut für Chemische Energiekonversion, D-45470 Mülheim, Germany*

Complete contact information is available at:
https://pubs.acs.org/10.1021/acs.jpcc.2c00174

■ REFERENCES

(1) Panov, G. I.; Dubkov, K. A.; Starokon, E. V. Active Oxygen in Selective Oxidation Catalysis. *Catal. Today* **2006**, *117*, 148−155.

(2) Freund, H.-J. Oxygen Activation on Oxide Surfaces: A Perspective at the Atomic Level. *Catal. Today* **2014**, *238*, 2−9.

(3) Hwang, J.; Rao, R. R.; Giordano, L.; Katayama, Y.; Yu, Y.; Shao-Horn, Y. Perovskites in Catalysis and Electrocatalysis. *Science* **2017**, *358*, 751−756.

(4) Adler, S. B. Factors Governing Oxygen Reduction in Solid Oxide Fuel Cell Cathodes. *Chem. Rev.* **2004**, *104*, 4791−4844.

(5) Gurlo, A. Interplay between O_2 and SnO_2: Oxygen Ionosorption and Spectroscopic Evidence for Adsorbed Oxygen. *ChemPhysChem* **2006**, *7*, 2041−2052.

(6) Schlögl, R. Heterogeneous Catalysis. *Angew. Chem., Int. Ed.* **2015**, *54*, 3465−3520.

(7) Haber, J.; Turek, W. Kinetic Studies as a Method to Differentiate between Oxygen Species Involved in the Oxidation of Propene. *J. Catal.* **2000**, *190*, 320−326.

(8) Rasmussen, M. D.; Molina, L. M.; Hammer, B. Adsorption, Diffusion, and Dissociation of Molecular Oxygen at Defected TiO_2(110): A Density Functional Theory Study. *J. Chem. Phys.* **2004**, *120*, 988−997.

(9) Ganduglia-Pirovano, M. V.; Hofmann, A.; Sauer, J. Oxygen Vacancies in Transition Metal and Rare Earth Oxides: Current State of Understanding and Remaining Challenges. *Surf. Sci. Rep.* **2007**, *62*, 219−270.

(10) Cui, Y.; Shao, X.; Baldofski, M.; Sauer, J.; Nilius, N.; Freund, H.-J. Adsorption, Activation, and Dissociation of Oxygen on Doped Oxides. *Angew. Chem., Int. Ed.* **2013**, *52*, 11385−11387.

(11) McFarland, E. W.; Metiu, H. Catalysis by Doped Oxides. *Chem. Rev.* **2013**, *113*, 4391−4427.

(12) Schwach, P.; Hamilton, N.; Eichelbaum, M.; Thum, L.; Lunkenbein, T.; Schlögl, R.; Trunschke, A. Structure Sensitivity of the Oxidative Activation of Methane over MgO Model Catalysts: II. Nature of Active Sites and Reaction Mechanism. *J. Catal.* **2015**, *329*, 574−587.

(13) Zasada, F.; Piskorz, W.; Janas, J.; Gryboś, J.; Indyka, P.; Sojka, Z. Reactive Oxygen Species on the (100) Facet of Cobalt Spinel Nanocatalyst and Their Relevance in $^{16}O_2/^{18}O_2$ Isotopic Exchange, deN$_2$O, and deCH$_4$ Processes—a Theoretical and Experimental Account. *ACS Catal.* **2015**, *5*, 6879−6892.

(14) Hävecker, M.; Wrabetz, S.; Kröhnert, J.; Csepei, L.-I.; Naumann d'Alnoncourt, R.; Kolen'ko, Y. V.; Girgsdies, F.; Schlögl, R.; Trunschke, A. Surface Chemistry of Phase-Pure M1Movtenb Oxide During Operation in Selective Oxidation of Propane to Acrylic Acid. *J. Catal.* **2012**, *285*, 48−60.

(15) Amakawa, K.; et al. How Strain Affects the Reactivity of Surface Metal Oxide Catalysts. *Angew. Chem., Int. Ed.* **2013**, *52*, 13553−13557.

(16) Davydov, A. A. *Molecular Spectroscopy of Oxide Catalyst Surfaces*; John Wiley & Sons Ltd.: Chichester, U.K., 2003.

(17) Wernbacher, A. M.; Kube, P.; Hävecker, M.; Schlögl, R.; Trunschke, A. Electronic and Dielectric Properties of MoV-Oxide (M1 Phase) under Alkane Oxidation Conditions. *J. Phys. Chem. C* **2019**, *123*, 13269−13282.

(18) Wernbacher, A. M.; Eichelbaum, M.; Risse, T.; Cap, S.; Trunschke, A.; Schlögl, R. Operando Electrical Conductivity and Complex Permittivity Study on Vanadia Oxidation Catalysts. *J. Phys. Chem. C* **2019**, *123*, 8005−8017.

(19) Koch, G.; et al. Surface Conditions That Constrain Alkane Oxidation on Perovskites. *ACS Catal.* **2020**, *10*, 7007−7020.

(20) Che, M.; Tench, A. J. Characterization and Reactivity of Mononuclear Oxygen Species on Oxide Surfaces. *Adv. Catal.* **1982**, *31*, 77−133.

(21) Che, M.; Tench, A. J. Characterization and Reactivity of Molecular Oxygen Species on Oxide Surfaces. *Adv. Catal.* **1983**, *32*, 1−148.

(22) Nováková, J. Isotopic Exchange of Oxygen ^{18}O between the Gaseous Phase and Oxide Catalysts. *Catal. Rev.* **1971**, *4*, 77−113.

(23) Choi, S. O.; Penninger, M.; Kim, C. H.; Schneider, W. F.; Thompson, L. T. Experimental and Computational Investigation of Effect of Sr on NO Oxidation and Oxygen Exchange for $La_{1-x}Sr_xCoO_3$ Perovskite Catalysts. *ACS Catal.* **2013**, *3*, 2719−2728.

(24) Winter, E. R. S. The Reactivity of Oxide Surfaces. *Adv. Catal.* **1958**, *10*, 196−241.

(25) Winter, E. R. S. Exchange Reactions of Oxides. Part IX. *J. Chem. Soc. A: Inorg., Phys., Theor.* **1968**, 2889−2902.

(26) Klier, K.; Nováková, J.; Jíru, P. Exchange Reactions of Oxygen between Oxygen Molecules and Solid Oxides. *J. Catal.* **1963**, *2*, 479−484.

(27) Boreskov, G. K. The Catalysis of Isotopic Exchange in Molecular Oxygen. *Adv. Catal.* **1965**, *15*, 285−339.

(28) Doornkamp, C.; Clement, M.; Gao, X.; Deo, G.; Wachs, I. E.; Ponec, V. The Oxygen Isotopic Exchange Reaction on Vanadium Oxide Catalysts. *J. Catal.* **1999**, *185*, 415−422.

(29) Doornkamp, C.; Clement, M.; Ponec, V. The Isotopic Exchange Reaction of Oxygen on Metal Oxides. *J. Catal.* **1999**, *182*, 390−399.

(30) Wachs, I. E.; Jehng, J.-M.; Deo, G.; Weckhuysen, B. M.; Guliants, V. V.; Benziger, J. B.; Sundaresan, S. Fundamental Studies of Butane Oxidation over Model-Supported Vanadium Oxide Catalysts: Molecular Structure-Reactivity Relationships. *J. Catal.* **1997**, *170*, 75−88.

(31) Klug, C. A.; Kroeker, S.; Aguiar, P. M.; Zhou, M.; Stec, D. F.; Wachs, I. E. Insights into Oxygen Exchange between Gaseous O_2 and Supported Vanadium Oxide Catalysts Via ^{17}O NMR. *Chem. Mater.* **2009**, *21*, 4127−4134.

(32) Avdeev, V. I.; Bedilo, A. F. Molecular Mechanism of Oxygen Isotopic Exchange over Supported Vanadium Oxide Catalyst VO_x/TiO_2. *J. Phys. Chem. C* **2013**, *117*, 2879−2887.

(33) Avdeev, V. I.; Bedilo, A. F. Electronic Structure of Oxygen Radicals on the Surface of VO_x/TiO_2 Catalysts and Their Role in

Oxygen Isotopic Exchange. *J. Phys. Chem. C* **2013**, *117*, 14701−14709.

(34) Koranne, M. M.; Goodwin, J. G.; Marcelin, G. Oxygen Involvement in the Partial Oxidation of Methane on Supported and Unsupported V_2O_5. *J. Catal.* **1994**, *148*, 378−387.

(35) Kera, Y.; Teratani, S.; Hirota, K. Infrared Spectra of Surface V═O Bond of Vanadium Pentoxide. *Bull. Chem. Soc. Jpn.* **1967**, *40*, 2458−2458.

(36) Hirota, K.; Kera, Y.; Teratani, S. Carbon Monoxide Oxidation with an Oxygen Tracer over a Vanadium Pentoxide Catalyst. *J. Phys. Chem.* **1968**, *72*, 3133−3141.

(37) Kera, Y.; Hirota, K. Infrared Spectroscopic Study of Oxygen Species in Vanadium Pentoxide with Reference to Its Activity in Catalytic Oxidation. *J. Phys. Chem.* **1969**, *73*, 3973−3981.

(38) Fletcher, W. H.; Rayside, J. S. High Resolution Vibrational Raman Spectrum of Oxygen. *J. Raman Spectrosc.* **1974**, *2*, 3−14.

(39) Pushkarev, V. V.; Kovalchuk, V. I.; d'Itri, J. L. Probing Defect Sites on the CeO_2 Surface with Dioxygen. *J. Phys. Chem. B* **2004**, *108*, 5341−5348.

(40) Choi, Y. M.; Abernathy, H.; Chen, H.-T.; Lin, M. C.; Liu, M. Characterization of O_2−CeO_2 Interactions Using in Situ Raman Spectroscopy and First-Principle Calculations. *ChemPhysChem* **2006**, *7*, 1957−1963.

(41) Wu, Z.; Dai, S.; Overbury, S. H. Multiwavelength Raman Spectroscopic Study of Silica-Supported Vanadium Oxide Catalysts. *J. Phys. Chem. C* **2010**, *114*, 412−422.

(42) Weckhuysen, B. M.; Jehng, J.-M.; Wachs, I. E. In Situ Raman Spectroscopy of Supported Transition Metal Oxide Catalysts: $^{18}O_2$−$^{16}O_2$ Isotopic Labeling Studies. *J. Phys. Chem. B* **2000**, *104*, 7382−7387.

(43) Lee, E. L.; Wachs, I. E. In Situ Raman Spectroscopy of SiO_2-Supported Transition Metal Oxide Catalysts: An Isotopic ^{18}O-^{16}O Exchange Study. *J. Phys. Chem. C* **2008**, *112*, 6487−6498.

(44) Moisii, C.; van de Burgt, L. J.; Stiegman, A. E. Resonance Raman Spectroscopy of Discrete Silica-Supported Vanadium Oxide. *Chem. Mater.* **2008**, *20*, 3927−3935.

(45) Magg, N.; et al. Vibrational Spectra of Alumina- and Silica-Supported Vanadia Revisited: An Experimental and Theoretical Model Catalyst Study. *J. Catal.* **2004**, *226*, 88−100.

(46) Döbler, J.; Pritzsche, M.; Sauer, J. Vibrations of Silica Supported Vanadia: Variation with Particle Size and Local Surface Structure. *J. Phys. Chem. C* **2009**, *113*, 12454−12464.

(47) Nitsche, D.; Hess, C. Normal Mode Analysis of Silica-Supported Vanadium Oxide Catalysts: Comparison of Theory with Experiment. *Catal. Commun.* **2014**, *52*, 40−44.

(48) Oyama, S. T.; Went, G. T.; Lewis, K. B.; Bell, A. T.; Somorjai, G. A. Oxygen Chemisorption and Laser Raman Spectroscopy of Unsupported and Silica-Supported Vanadium Oxide Catalysts. *J. Phys. Chem.* **1989**, *93*, 6786−6790.

(49) Ono, T.; Tanaka, Y.; Takeuchi, T.; Yamamoto, K. Characterization of K-Mixed V_2O_5 Catalyst and Oxidative Dehydrogenation of Propane on It. *J. Mol. Catal. A Chem.* **2000**, *159*, 293−300.

(50) Ono, T.; Numata, H. Characteristic Features of Raman Band Shifts of Vanadium Oxide Catalysts Exchanged with the ^{18}O Tracer and Active Sites for Reoxidation. *J. Mol. Catal. A Chem.* **1997**, *116*, 421−429.

(51) Browne, M. P.; Sofer, Z.; Pumera, M. Layered and Two Dimensional Metal Oxides for Electrochemical Energy Conversion. *Energy Environ. Sci.* **2019**, *12*, 41−58.

(52) Wachs, I. E. Recent Conceptual Advances in the Catalysis Science of Mixed Metal Oxide Catalytic Materials. *Catal. Today* **2005**, *100*, 79−94.

(53) Grant, J. T.; Venegas, J. M.; McDermott, W. P.; Hermans, I. Aerobic Oxidations of Light Alkanes over Solid Metal Oxide Catalysts. *Chem. Rev.* **2018**, *118*, 2769−2815.

(54) Kuba, S.; Knözinger, H. Time-Resolved in Situ Raman Spectroscopy of Working Catalysts: Sulfated and Tungstated Zirconia. *J. Raman Spectrosc.* **2002**, *33*, 325−332.

(55) Giannozzi, P.; et al. Quantum Espresso: A Modular and Open-Source Software Project for Quantum Simulations of Materials. *J. Phys.: Condens. Matter* **2009**, *21*, 395502.

(56) Shklover, V.; Haibach, T.; Ried, F.; Nesper, R.; Novák, P. Crystal Structure of the Product of Mg^{2+} Insertion into V_2O_5 single Crystals. *J. Solid State Chem.* **1996**, *123*, 317−323.

(57) Grimme, S. Semiempirical Gga-Type Density Functional Constructed with a Long-Range Dispersion Correction. *J. Comput. Chem.* **2006**, *27*, 1787−1799.

(58) Barone, V.; Casarin, M.; Forrer, D.; Pavone, M.; Sambi, M.; Vittadini, A. Role and Effective Treatment of Dispersive Forces in Materials: Polyethylene and Graphite Crystals as Test Cases. *J. Comput. Chem.* **2009**, *30*, 934−939.

(59) Monkhorst, H. J.; Pack, J. D. Special Points for Brillouin-Zone Integrations. *Phys. Rev. B* **1976**, *13*, 5188−5192.

(60) Kim, H.; Kosuda, K. M.; Van Duyne, R. P.; Stair, P. C. Resonance Raman and Surface- and Tip-Enhanced Raman Spectroscopy Methods to Study Solid Catalysts and Heterogeneous Catalytic Reactions. *Chem. Soc. Rev.* **2010**, *39*, 4820−4844.

(61) Harima, H. Raman Scattering Characterization on SiC. *Microelectron. Eng.* **2006**, *83*, 126−129.

(62) Gilson, T. R.; Bizri, O. F.; Cheetham, N. Single-Crystal Raman and Infrared Spectra of Vanadium(V) Oxide. *J. Chem. Soc., Dalton Trans.* **1973**, 291−294.

(63) Abello, L.; Husson, E.; Repelin, Y.; Lucazeau, G. Vibrational Spectra and Valence Force Field of Crystalline V_2O_5. *Spectrochim. Acta, Part A* **1983**, *39*, 641−651.

(64) Clauws, P.; Broeckx, J.; Vennik, J. Lattice Vibrations of V_2O_5. Calculation of Normal Vibrations in a Urey-Bradley Force Field. *Phys. Status Solidi B* **1985**, *131*, 459−473.

(65) Brázdová, V.; Ganduglia-Pirovano, M. V.; Sauer, J. Periodic Density Functional Study on Structural and Vibrational Properties of Vanadium Oxide Aggregates. *Phys. Rev. B* **2004**, *69*, 165420.

(66) Zhou, B.; He, D. Raman Spectrum of Vanadium Pentoxide from Density-Functional Perturbation Theory. *J. Raman Spectrosc.* **2008**, *39*, 1475−1481.

(67) Wu, Z.; Kim, H.-S.; Stair, P. C.; Rugmini, S.; Jackson, S. D. On the Structure of Vanadium Oxide Supported on Aluminas: UV and Visible Raman Spectroscopy, UV−Visible Diffuse Reflectance Spectroscopy, and Temperature-Programmed Reduction Studies. *J. Phys. Chem. B* **2005**, *109*, 2793−2800.

(68) Hermann, K.; Witko, M.; Druzinic, R.; Tokarz, R. Hydrogen Assisted Oxygen Desorption from the V_2O_5(010) Surface. *Top. Catal.* **2000**, *11/12*, 67−75.

(69) Huang, Y.-L.; Pellegrinelli, C.; Wachsman, E. D. Reaction Kinetics of Gas−Solid Exchange Using Gas Phase Isotopic Oxygen Exchange. *ACS Catal.* **2016**, *6*, 6025−6032.

(70) Huang, Y.-L.; Pellegrinelli, C.; Sakbodin, M.; Wachsman, E. D. Molecular Reactions of O_2 and CO_2 on Ionically Conducting Catalyst. *ACS Catal.* **2018**, *8*, 1231−1237.

(71) Huang, Y.-L.; Pellegrinelli, C.; Wachsman, E. D. Oxygen Dissociation Kinetics of Concurrent Heterogeneous Reactions on Metal Oxides. *ACS Catal.* **2017**, *7*, 5766−5772.

(72) Tilley, R. J. *Understanding Solids: The Science of Materials*; Wiley: 2013.

(73) Cameron, W. C.; Parkas, A.; Litz, L. M. Exchange of Isotopic Oxygen between Vanadium Pentoxide, Gaseous Oxygen and Water. *J. Phys. Chem.* **1953**, *57*, 229−238.

(74) Milan, E. F. The Dissociation Pressure of Vanadium Pentoxide. *J. Phys. Chem.* **1929**, *33*, 498−508.

(75) Nasu, N. The Dissociation Pressure of Vanadium Pentoxide. *J. Chem. Soc. Jpn.* **1935**, *56*, 666−669.

(76) Spitsyn, B. N.; Maidanovskaya, L. L. The Thermal Dissociation of Vanadium Pentoxide. *Zh. Fiz. Khim.* **1959**, *33*, 180−183.

(77) Chen, K.; Khodakov, A.; Yang, J.; Bell, A. T.; Iglesia, E. Isotopic Tracer and Kinetic Studies of Oxidative Dehydrogenation Pathways on Vanadium Oxide Catalysts. *J. Catal.* **1999**, *186*, 325−333.

(78) Ma, W. Y.; Zhou, B.; Wang, J. F.; Zhang, X. D.; Jiang, Z. Y. Effect of Oxygen Vacancy on Li-Ion Diffusion in a V_2O_5 Cathode: A First-Principles Study. *J. Phys. D Appl. Phys.* **2013**, *46*, 105306.

(79) Mars, P.; van Krevelen, D. W. Oxidations Carried out by Means of Vanadium Oxide Catalysts. *Chem. Eng. Sci.* **1954**, *3*, 41−59.

(80) Routray, K.; Reddy, K. R. S. K.; Deo, G. Oxidative Dehydrogenation of Propane on V_2O_5/Al_2O_3 and V_2O_5/TiO_2 Catalysts: Understanding the Effect of Support by Parameter Estimation. *Appl. Catal. A Gen.* **2004**, *265*, 103−113.

(81) Alexopoulos, K.; Reyniers, M.-F.; Marin, G. B. Reaction Path Analysis of Propane Selective Oxidation over V_2O_5 and V_2O_5/TiO_2. *J. Catal.* **2012**, *289*, 127−139.